Journal of Material Chemistry A

ARTICLE

In operando XAS investigation of reduction and oxidation processes in cobalt and iron mixed spinels during the chemical loop reforming of ethanol

F. Carraro,[a,†] O. Vozniuk,[b,†] L. Calvillo,[a] L. Nodari,[c] C. La Fontaine,[d] F. Cavani,[b] S. Agnoli*[,a]

FeCo$_2$O$_4$ and CoFe$_2$O$_4$ nanoparticles have been studied as oxygen carriers for the Chemical Loop Reforming (CLR) of ethanol. By using *in operando* x-ray absorption spectroscopy we have followed in real time the chemical and structural changes that take place on the materials as a function of temperature and reactive atmosphere (i.e. ethanol/ water streams). During the first step of CLR for both oxides the most active chemical species are the cations in the tetrahedral sites, disregarding of their chemical nature. Quite rapidly the spinel structure is transformed into a mix of wüstite-type oxide and metal alloy, but the formation of a metal phase is easier in the case of cobalt, while iron shows a marked preference to form wüstite type oxide. Despite the good reducibility of FeCo$_2$O$_4$ imparted by the high amount of cobalt, its performance in the production of hydrogen is quite poor due to an inefficient oxidation by water steam, which is able to oxidize only the outer shell of the nanoparticles. On the contrary CoFe$_2$O$_4$ due to the residual presence of a reducible wüstite phase shows a higher hydrogen yield. Moreover, by connecting the structural information provided by x-ray absorption spectroscopy with the analysis of the byproducts of ethanol decomposition we could infer that FeCo$_2$O$_4$ is more selective than CoFe$_2$O$_4$ for the selective dehydrogenation of ethanol to acetaldehyde because of the higher amount of Fe(III) ions in tetrahedral sites.

Introduction

Metal oxides have always held a strong position in catalysis given their wide use as supports, promoters, and active phases.[1,2] Quite recently though, the interest for these materials have increased even more because they perfectly satisfy the stringent requirements enforced by the new standards of sustainability and environmental "greenness"[3] of modern chemistry.[4] This has stimulated the scientific community to look for new oxides with special structural and chemical properties that are optimized for specific catalytic applications.[5] In this context, complex oxides i.e. compounds containing several types of metal cations in different structural environments, represent ideal candidates for the development of advanced materials with easily tunable multifunctional properties.[2,6] Among these, a central spot is occupied by the large family of spinels, which are crystalline oxides characterized by excellent stability associated with high structural flexibility.[7,8]

Spinels have general formula AB$_2$O$_4$ and are constituted by a close packed lattice of face centered cubic oxygen anions, where the resulting tetrahedral and octahedral holes can be variably filled by metal cations in such a way that the overall electroneutrality of the system is maintained.[9] In their simplest and most typical form, spinels are formed by divalent and trivalent cations in a 1:2 ratio, however almost any type of cation combination, encompassing also monovalent and tetravalent ions in the right stoichiometry, can be fitted into the structure. This gives access to the preparation of a wide range of oxide materials that exhibit a large gamut of different physicochemical properties. Nonetheless, the huge potential of spinels, inherent to their structural and chemical versatility, has been only partially exploited in practical applications because of a limited understanding of very fundamental processes such as their oxidation/reduction or phase transitions and their dynamic behavior *in operando* conditions.[10]

From the chemical point of view, spinels exhibit a quite fascinating acid-base and redox activity, which play a key role in several catalytic reactions involving oxygen species and in electrocatalysis.[2,8] As a matter of fact, these oxides may present Brønsted or Lewis acid (i.e. undercoordinated surface cations) and basic sites (i.e. surface hydroxyls and oxygen species). Moreover, according to the nature of the cations, they can host a variety of redox couples (e.g. Fe(II)/Fe(III) or Co(II)/Co(III)).

Unfortunately, such versatility and flexibility come at a price of high complexity, so a high level of empiricism characterizes this field. A substantial gap of knowledge still prevents a rational design of spinel materials for specific catalytic applications.

Recently however, due to the development of advanced *in operando* techniques, it has been possible to obtain an exceptionally detailed understanding about the structure/activity correlation in these materials. As an example,

a. Department of Chemical Science, University of Padova, via Marzolo 1, Padua 35131, Italy. email: stefano.agnoli@unipd.it
b. Dipartimento di Chimica Industriale "Toso Montanari", Università di Bologna, Viale del Risorgimento, 4, 40136 Bologna, Italy.
c. Istituto di Chimica della Materia Condensata e di Tecnologie per l'Energia, CNR-ICMATE and INSTM, via Marzolo 1, Padua 35131, Italy.
d. Synchrotron SOLEIL, L'Orme des Merisiers, 91190 Saint-Aubin, France
† These authors contributed equally

it has been shown by X-ray absorption spectroscopy (XAS), that the high chemical reactivity observed in Mn based spinel catalysts in the oxygen evolution reaction and oxygen evolution reaction can be traced back to Mn in octahedral sites.[11] On the other hand, in the field of gas-phase heterogeneous catalysis, it has been demonstrated by *in situ* Diffuse Reflectance Infrared Fourier Transform Spectroscopy (DRIFTS) combined with x-ray absorption spectroscopy (XAS) and Raman spectroscopy, that octahedrally coordinated Co(II) sites are more easily oxidized to Co(III) in comparison with Co(II) in tetrahedral site, and Co(III) species are the active centers for the oxidation of organic volatile compounds.[12]

These results highlight the great interest for understanding the interplay between geometrical (e.g. tetrahedral vs octahedral occupancy) and chemical factors (e.g. oxidation state) to determine the final reactivity of materials.

In the present work, we decided to investigate two exemplary mixed Co-Fe spinels, the cobalt rich iron cobaltite ($FeCo_2O_4$) and the iron rich cobalt ferrite ($CoFe_2O_4$). This latter has demonstrated to be an extremely interesting material for electrocatalysis,[13,14] oxidation reactions,[15,16] and as oxygen or electron carriers[17] for a two steps Chemical Loop Reforming (CLR).[18,19,20,21] On the contrary, very few works are focused on $FeCo_2O_4$ and its potential in catalysis still is largely untapped.[22,23,24]

CLR represents a potentially carbon neutral process for the production of high purity hydrogen. It is based on a dual thermal redox cycle. At first the oxide material is exposed to reducing atmosphere to obtain highly reduced phases and then to steam for its reoxidation and consequent formation of H_2.[25]

We have focused our attention on the use of ethanol as reducing agent.[26] This choice is quite appealing because ethanol is a not toxic, low cost, fuel that can be easily obtained from renewable sources and on the other hand Co-Fe mixed spinel are abundant and cheap materials with a low environmental impact. CLR of ethanol on spinels therefore has a great potential for the sustainable production of hydrogen.

By a combination of different *in situ* characterization techniques and catalytic measurements we have investigated the structural and chemical properties of these mixed Co-Fe spinels during each step of the CLR of ethanol. For the first time, we were able to follow in real time, the reduction process of mixed spinels, monitoring the formation of a series of reduced phases. We were also able to identify which are the most chemically active cations inside the spinel structure and what are the parameters that control the chemical activity toward ethanol.

The fundamental knowledge acquired in this study may be a stepping stone for the design of new improved materials to be used as solid oxygen carriers and novel catalysts for the selective oxidation of alcohols.

Results and Discussion

In this work, we have focused our attention on the two end members of the family of mixed Fe-Co spinel oxides: $CoFe_2O_4$ (cobalt ferrite) and $FeCo_2O_4$ (iron cobaltite) that were prepared

by a simple precipitation route from aqueous solution (see SI for details about the synthesis).

Characterization of as-prepared catalysts.

Combining X-ray Diffraction (XRD), Raman spectroscopy, Energy Dispersive X-ray spectroscopy (EDX), Mössbauer and X-ray Absorption Spectroscopy (XAS), we have determined the structure and the chemical composition of the two samples.

Fig. 1b shows the XRD data for the two Co-Fe oxides. The pattern of $CoFe_2O_4$ shows the typical reflections of magnetite (Fe_3O_4), as reported in our previous papers[27] Similarly, the diffraction data of $FeCo_2O_4$ indicate the formation of a spinel structure.[28,29] No other phases are observed, confirming that a homogeneous and highly crystalline $FeCo_2O_4$ phase is formed at the synthesis temperature (i.e. 450°C for $CoFe_2O_4$ and 900ºC $FeCo_2O_4$). As a consequence of the elevated calcination temperature, the iron cobaltite exhibits lower specific surface area (4 m^2 g^{-1}) and larger crystallite size (32 nm) than cobalt ferrites (12 nm crystallite size, 69 m^2 g^{-1} surface area) (see Table S1). The spinel structure of both samples is also confirmed by the Raman spectra reported in Fig. 1a. Vibrational spectroscopy is a powerful technique for the structural analysis of spinel oxides, since their spectroscopic fingerprint is highly specific, and strongly affected by stoichiometry, cation distribution, and defects. The Raman spectra of spinels are generally complex and show more Raman-active modes than those predicted by group theory: $F_{2g}(1)$, E_g, $F_{2g}(2)$, $F_{2g}(3)$ and A_{1g}. The additional vibrations may appear because of local distortions of the crystal lattice. These defects do not affect the long range order of the system, and often cannot be directly detected by XRD. The strong intensity and sharpness of the bands in the $FeCo_2O_4$ spectrum confirm the high crystallinity of the sample. Five main vibration modes are observed at 192, 479, 507, 598 and 673 cm^{-1}, the latter showing a shoulder at about 645 cm^{-1}. The most intense vibration modes are related to MO_4 (the peak at 673 cm^{-1} and its shoulder) and MO_6 stretching (at 192 cm^{-1}). The $CoFe_2O_4$ spectrum presents six vibration modes, as already reported in the literature.[30] The five first order Raman modes can be observed at about 182, 306, 476, 562, 636 and 690 cm^{-1}. The intense vibration modes at 636 and 690 cm^{-1} are the $A_{1g}(2)$ and $A_{1g}(1)$, respectively, which can be assigned to the MO_4 stretching vibrations and to the disorder effect of Co(II) and Fe(III) over the T_d and O_h sites.[30,31]

The oxidation state and site occupancy of the metal species in the spinel structure were determined by ex-situ XAS.[32,33,34] In transition metals K-edges, XANES transitions involve the excitation of a 1s photoelectron into a mainly 4p derived continuum of states. In general, when the valence of the absorbing metal atom is increased (i.e the metal is present in a higher oxidation state), a shift of the absorption edge toward higher energy is observed. XANES and Fourier Transform (FT) EXAFS spectra for the Co-Fe spinels are shown in Fig. 1 c,d,e,f. Comparing the energy position of the absorption edge in the XANES spectra with that of the reference samples, it is possible to determine with great accuracy the oxidation state of each element in the spinel structure (Fig. 1 c,d,e,f). In $CoFe_2O_4$, the oxidation state of Fe and Co is close to +3 and +2, respectively, as expected;[32] whereas in $FeCo_2O_4$, the oxidation state for Fe
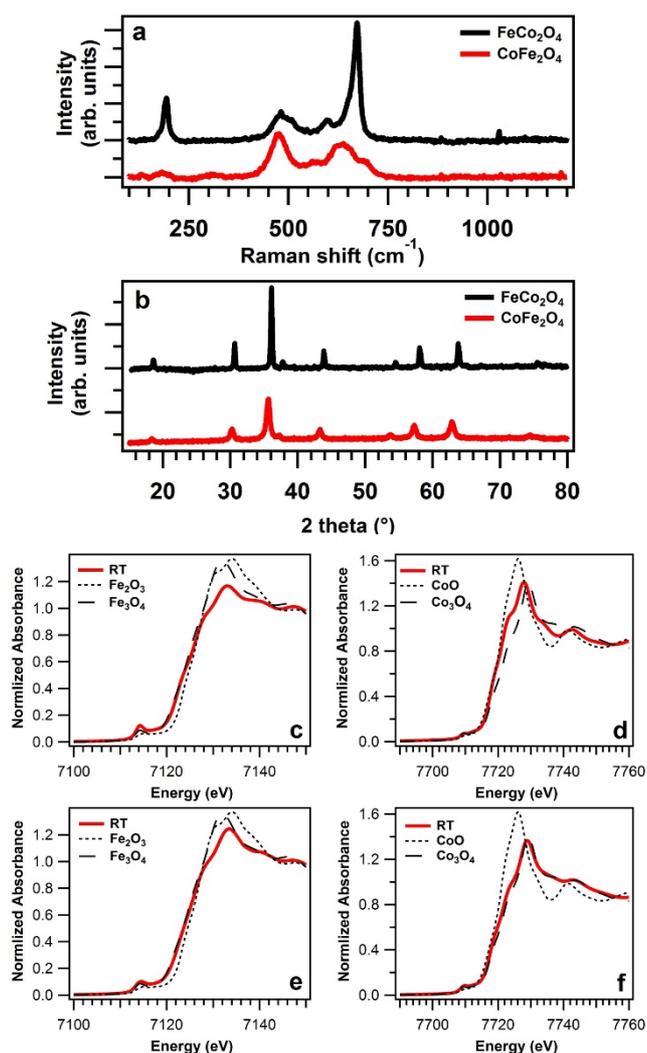
Fig. 1 *Raman spectra (a) and XRD patterns of as prepared materials; XANES spectra at Fe(c,e) and Co (d,f) K-edge for as prepared $CoFe_2O_4$ (c,d), $FeCo_2O_4$ (e,f) and reference compounds.*

and Co are +3 and +2/+3, respectively. Moreover, the fine structure of the pre-edge can provide further information about the structure of spinels.[32,33,34] At K-edges in fact, pre-edge peaks, which correspond to 1s → 3d transitions (with 3d-4p mixing), may occur at about 15-20 eV before the white line. An increase of the intensity of these features corresponds to the removal of the inversion symmetry in the environment of the absorbing atom. Therefore, the pre-edge feature can provide a direct indication whether a metal center is located in a tetrahedral or octahedral site. At the Co K-edge, the pre-edge peak intensity of cobaltite is higher than that of ferrite, indicating that the cobaltite contains a higher amount of tetrahedrally coordinated Co ions. Conversely, the Fe K-edge pre-peak intensity is higher in the $CoFe_2O_4$ sample. The cation distribution was determined by EXAFS data of the starting materials.[32,34] The crystallographic site occupancy in spinels is defined by the inversion parameter γ, i.e. the fraction of tetrahedral sites occupied by majority ions.[9] The best fits of the FT EXAFS data are reported in Fig. S1 and S2 and the

corresponding parameters are reported in Tables S3 and S4. At Fe K-edge, the first peak at about 2 Å (not phase-corrected) is due to the contribution of two Fe-O single scattering paths: Fe_{Tetra}-O and Fe_{Octa}-O, which correspond to the interatomic distances between the two first coordination shells of oxygen ions, respectively. In the region between 2.0 and 3.5 Å, two contributions are observed, one at around 2.5 Å is related to Fe_{Octa}-M_{Octa} (M=Fe, Co) scattering paths and another one at about 3.5 Å to Fe_{Tetra}-M_{Tetra} or Fe_{Tetra}-M_{Octa} interactions. In fact, due to the similar cross sections, from EXAFS spectra it is not possible to distinguish between Fe and Co as backscattering atom. The EXAFS spectra at Co K-edge can be interpreted along the same line as well. An inversion degree of 0.8 and 0.6 was calculated for $CoFe_2O_4$ and $FeCo_2O_4$, respectively. These values are in agreement with previously reported data.[28] Therefore, the cation distribution can be summarized as:

$FeCo_2O_4$: $[Co(II)_{0.6}Fe(III)_{0.4}]^{Tet}[Co(II)_{0.4}Fe(III)_{0.6}Co(III)_1]^{Oct}O_4$

$CoFe_2O_4$: $[Co(II)_{0.2}Fe(III)_{0.8}]^{Tet}[Co(II)_{0.8}Fe(III)_{1.2}]^{Oct}O_4$
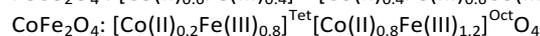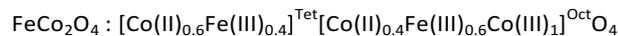
The results obtained by EXAFS were further verified by Mössbauer spectroscopy measurements, which were taken both at RT and 80 K.

Concerning $FeCo_2O_4$, RT spectra shows a broad magnetic pattern (Fig. 2a) as results of the magnetic relaxation due to high ordering temperature.[28] On the contrary, $CoFe_2O_4$, shows a fully magnetically ordered RT spectrum. (Fig. 2b). No traces of superparamagnetic components are detectable. A preliminary fit excluded the presence of pure Fe(III) oxides, such as hematite. After cooling down the $FeCo_2O_4$ sample to 80 K, the spectrum transforms into a well-defined magnetic pattern (Fig. 2c), typical of Fe species in a spinel structure. As explained in the Experimental Section, the spectrum was fitted by using only two broad sextets. The so-obtained parameters were attributable to Fe(III) in tetrahedral and octahedral environment, whose relative areas are 44 and 56 respectively. Therefore, cation distribution within the spinel structure is similar to that suggested by EXAFS data, and the cobaltite can be written as: $[Co_{0.56}Fe(III)_{0.44}]^{Tet}[Co_{1.44}Fe(III)_{0.56}]^{Oct}O_4$.

Concerning the $CoFe_2O_4$ sample, the spectrum acquired at 80 K (Fig. 2d) was firstly fitted by using two sextets, relative to the octahedral and tetrahedral site. The tetrahedral and octahedral populations were estimated respectively in 37 and 63 of the total Fe. Once again, assuming γ= 0.37, the stoichiometry of the spinels is in good agreement with the EXAFS data, in fact the proposed formula is $Co_{0.26}Fe(III)_{0.74}]^{Tet}[Co_{0.74}Fe(III)_{1.26}]^{Oct}O_4$. The small discrepancy in the so calculated stoichiometry can be ascribed either to small errors in the area calculation or to small differences in the recoilless fraction of the two different sites.

In both cases, the proposed fitting highlights the linewidth broadening due to the effect of a multiplicity of hyperfine magnetic fields on the Fe(III) nuclei. If the contribution of the Near Next Neighbors (NNN) on the tetrahedral site can be
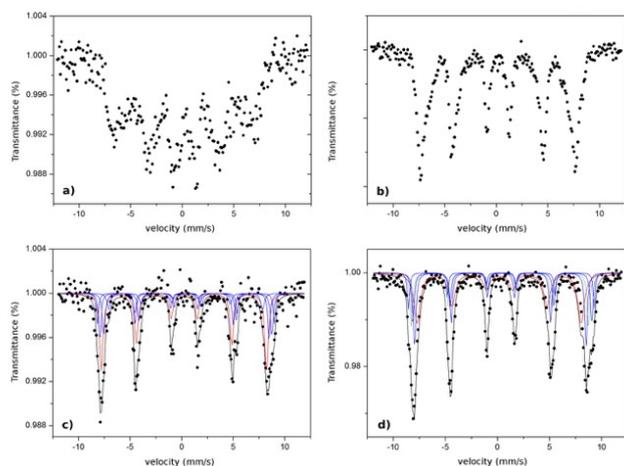
Fig. 2 Mössbauer spectra of $FeCo_2O_4$ and Co_2FeO_4, collected at RT, a) and b), and at 80 K, c) and d). Black dots represent the experimental data, black lines the calculated spectra, red line the Fe(III) tetrahedral site and blue lines the sub-components of the octahedral site.

Fig. 3 Oxidation states calculated from the edge position in the XANES spectra collected during the annealing treatment in reductive atmosphere (0.69 % ethanol in N_2).

neglected,[35] on the contrary on the octahedral sites it needs to be taken in account.

Therefore, by using the binomial distribution described in the Experimental Section, the proper number of subcomponents and their relative areas can be obtained. Considering negligible the areas smaller than 5% of the total iron, the binomial distribution on the octahedral sites in iron cobaltite predicts the presence of four sextets, whose relative areas are given by P(4):P(3):P(2):P(1)=18:30:29:16. Also in cobalt ferrite, the binomial distribution predicts four sextets, with an intensity ratio of P(4):P(3):P(2):P(1)=11:25:33:22. The intensity of the sextets were recalculated on the basis of the total area of the octahedral site and fixed during the fitting procedure. The parameters are reported in table S5, supplementary materials. These differences in NNN configuration reflect the different γ in the two spinels, that is the different statistic distributions of Co atoms in the cobaltite and ferrite structures.

In operando XAS: annealing in reductive atmosphere

Freshly prepared $FeCo_2O_4$ and $CoFe_2O_4$ spinel oxides were evaluated as electrons/O^{2-} carrier materials for hydrogen production via CLR of ethanol. The changes of the materials during the redox cycle were followed *in real time* by XAS measurements in order to determine the reactivity of the two metal ions in the different geometrical-sites. As first step, we investigated the reaction of the materials toward ethanol as a function of temperature. *In operando* XAS was performed during the annealing of the samples from RT to 500°C in reducing atmosphere (0.69% vol of ethanol in N_2). Fig. 3 reports the variation of the mean oxidation state of Fe and Co determined from the edge position as a function of temperature. The change of the average oxidation state of the cations was calculated by XANES spectra (Fig. S3), whereas modifications in the geometric site were deduced by the EXAFS data (Fig. 4). The body of our experimental data outlines a marked difference of reducibility in the two spinels. $FeCo_2O_4$ is stable up to 350°C, above this temperature it starts to reduce quickly, and at 425°C the material is mainly made up by the corresponding body centered cubic (bcc) metal alloy phases, as
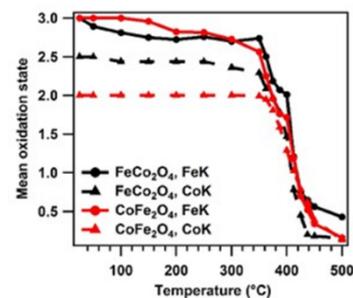
suggested by the spectral fingerprint of FT EXAFS spectra (Fig. S6) and by the XRD patterns of the reduced samples (Fig. S7).[36] Moreover, several works indicate that alloys are the most stable phases formed under reducing condition for mixed ferrites.[37,38] $CoFe_2O_4$ shows a similar behavior, although the reduction is more gradual: Fe starts to reduce at 150°C and becomes metal Fe at 500ºC, whereas Co is stable up to 250 ºC and then it is gradually reduced to metal Co. It has to be noted however, that the higher reducibility of $CoFe_2O_4$ can be also due to the higher surface area and defectivity of this material. In order to investigate the effect of cation site occupancy in the two spinels, we carefully analyzed the intensity trends of the EXAFS peaks (Fig. 4) and of the LCF of XANES spectra (Fig. 5) in $CoFe_2O_4$ and $FeCo_2O_4$ during the thermal treatment in presence of ethanol. From these data a general behavior of the reduction mechanism is deduced, which appears to be largely controlled by the type of cation coordination. The cations in tetrahedral
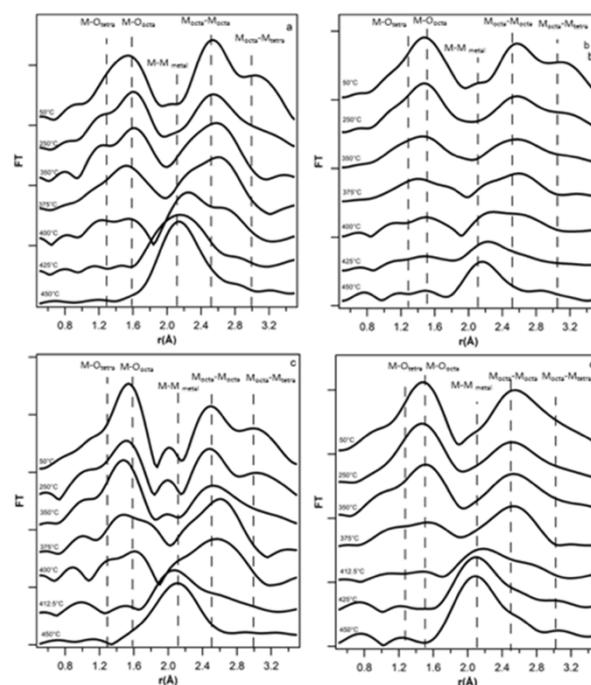

Fig. 4 Fourier transform EXAFS spectra at Co K(a,c) and Fe K (b,d) edge for $CoFe_2O_4$ (a,b), $FeCo_2O_4$ (c,d) during the annealing treatment in reductive atmosphere (0.69 % ethanol in N_2).
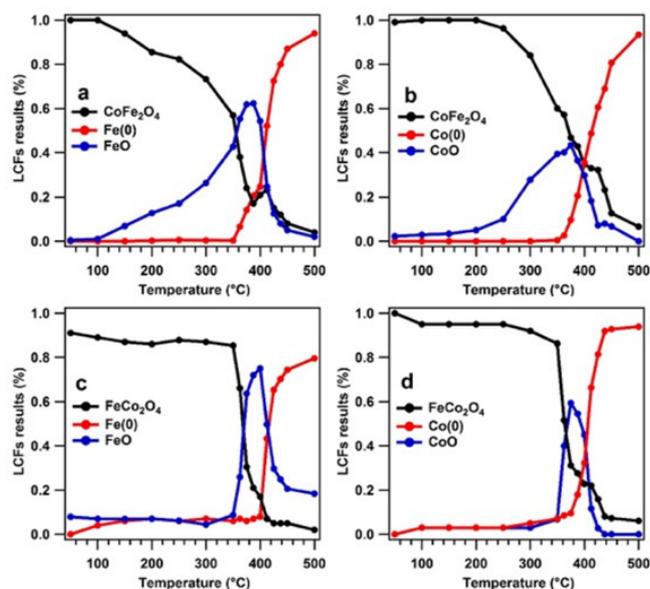
Fig. 5 LCFs (% of composition vs temperature) of Fe(a,c) and Co (b,d) K-edge for $CoFe_2O_4$ (a,b) and $FeCo_2O_4$ (c,d) during the annealing treatment in reducing atmosphere (0.69 % ethanol in N_2)

sites (A) are more prone to reduction than those in octahedral sites (B). This is evidenced by the decrease of the peak corresponding to M_{Octa}-M_{Tetra} bonds until its complete suppression at about 350°C, whereas the M_{Octa}-M_{Octa} peak intensity decreases only slightly. Combining the EXAFS data with the LCF analysis at the Fe K and Co K edges (Fig. 5), it can be concluded that the disappearance of the M_{Octa}-M_{Tetra} peak is related to the formation of M(II) oxide phases, probably a mixed $(Fe,Co)O_{1-x}$, wüstite (as suggested also by the XRD patterns acquired on the reduced samples, Fig. S6). In the case of $FeCo_2O_4$, the maximum conversion to M(II) oxides is reached at 400°C, whereas in the case of $CoFe_2O_4$ at 375°C. These M(II) oxides are highly disordered, also in the short range order, since no clear EXAFS peaks can be identified. Only in the case of majority cations of the spinels (B cations, i.e. Fe in ferrite and Co in cobaltite), the growth of a shoulder related to M-O bonds typical of wüstite structures is identified at 1.7 Å, starting from 375-400°C. The higher activity of tetrahedral sites is somehow in contrast with a previous report about the reactivity of mixed ferrites toward methanol, where by ex situ characterization it was suggested a higher activity of octahedral sites,[39] however it is in agreement with other investigations on the reaction mechanism of spinel.[40,41] As a matter of fact, Mössbauer experiments suggest that during the thermal or chemical reduction of ferrites, the removal of oxygen induces a change in the oxidation state of cations that therefore adjust their site occupancy, by populating interstitial sites:[41] i.e. sites that are not normally occupied in the parent structures, however the structural details of such processes are strongly dependent on the specific oxide structures. Our XAS data therefore, for the first time capture time resolved snapshots of tetrahedral cations diffusion into normally unoccupied octahedral sites forming cation excessive[40] spinels, which at the limit of high reduction are eventually converted to wüstite type oxides. Comparing the two oxides, $FeCo_2O_4$ seems to be more stable

toward reduction than $CoFe_2O_4$, as evidenced by the higher temperature needed to reduce the signals coming from the spinel. However, the higher stability may be due to the larger size and low surface area of iron cobaltite nanoparticles that prevent a fast surface reaction. On the other hand, $CoFe_2O_4$ shows an almost immediate conversion to the wüstite phases. The fast reaction, characterized by an almost linear kinetics as a function of time, suggests that intrinsic defects play a key role in the reduction. At high temperatures (> 350°C), the wüstite phases and the residual ferrite/cobaltite are mostly converted to metal phases. From the LCF analysis, it is clear that the formation of the metal phases starts only when a relatively large amount of (Co, Fe) mixed wüstite is formed; therefore, a direct decomposition of the spinel to the metal seems unlikely. In general, the reduction of ferrites follows a path that is strongly dependent on the type of reducing agent (H_2, CO, alcohols), temperature, but also morphological factors.[42] In the case of the Fe_3O_4 it has been determined by thermodynamic data,[43] that a triple point exist at 1121 K where Fe_3O_4, FeO, Fe coexist, whereas for lower temperature Fe_3O_4 is directly converted to metal Fe. This prediction has been later verified experimentally in the experimental work of Bohn et al.[44] On other hand, for several spinel ferrites it has been reported an easy and direct formation of metal phases: for example, $NiFe_2O_4$ is directly reduced at 850°C by simulated biomass pyrolysis gas to a metal Nickel phase and Fe_3O_4.[45] Similarly, accurate experimental and theoretical investigations suggest that during the reduction with syngas, only in the limit of very low (<0.03) CO/CO_2 and H_2/H_2O ratios, CoO and NiO are formed from Co,Ni mixed ferrites, otherwise a direct decomposition to metal Ni and Co and iron enriched spinel is observed.[20] More recently, in the case of the reduction of cobalt ferrites, at 600°C by a mixture of syngas and CO_2 no trace of wüstite phase was observed by *in situ* XRD, but only a direct conversion of mixed spinel to a Co-Fe metal alloy.[18] Anyway all the reports in the literature suggest that the introduction of Co, Ni, and other first row transition metal cations facilitates the reduction of both the parent spinel Co_3O_4 and Fe_3O_4.[29,46] Our *in operando* results therefore outline a different scenario that clearly points to the formation of a large fraction of intermediate wüstite phases even at very modest temperature. It is also interesting to note that the presence of metal Fe in $FeCo_2O_4$ is observed only at temperatures higher than 400°C, which is a much higher temperature than that required for the formation of metal Co in the same material or metal Fe in $CoFe_2O_4$. As a matter of fact, the strength of Co-O bonds is smaller than Fe-O and one of the lowest among first row transition metal oxides,[7] and in general the introduction of Co in iron spinel has the effect to promote reducibility. This is in agreement with previous TPR measurements and reactivity studies toward methanol[29] and suggest that not only the chemical composition, but also structural factors are very important to understand the reactivity of mixed oxides. Finally, the analysis of the M-O peak intensity (1.2-1.6 Å) indicates that the A cations are fully reduced at temperature lower than that for the B cations in both samples (Fe in $FeCo_2O_4$ and Co in $CoFe_2O_4$). Notably, the LCF analysis suggests that single metal spinels (Co_3O_4 or Fe_3O_4)

are not \formed in any of the materials during the annealing in ethanol.

CLR of ethanol: catalytic tests

Bearing in mind these results, we tested the redox and catalytic properties of these materials with respect to the two-step CLR of ethanol at two different temperatures: at 350°C, because this is the threshold for the reduction of the catalysts; and at 450°C, because at this temperature both spinels are mostly reduced to a metal phase. Previously, the catalytic properties of $M_xFe_yO_4$ spinels as catalyst for CLR at 450°C were investigated by Vozniuk et al.[27] In the CLR process, the first step is the aerobic oxidation of ethanol, whereas the second one is the reoxidation of the catalyst by water vapor exposure.

Considering that the anaerobic oxidation is a stoichiometric process, the reduction state of the material is pivotal in determining the selectivity of the reaction path. Therefore, the temperature has a major role in this reaction. The amount of each reaction product is affected by the extent of the metal oxide reduction, which is a general statement valid for all oxygen carrier materials.[21]

During the reduction step performed at 350°C for 20 min, the ethanol conversion and the selectivity to the main products were determined by gas chromatography (on-line micro-GC). The ethanol conversion over $FeCo_2O_4$ (Fig. S8) and $CoFe_2O_4$ (Fig. S9) is 18% and 20%, respectively. The main products formed during the reaction were identified as follows: acetaldehyde, ethyl acetate, acetone, H_2O, CO_2, H_2, ethylene and ethane. Acetaldehyde is the predominant product for $FeCo_2O_4$ with an initial selectivity of about 69 %, (which decreases to 57% at the end of the cycle). On the other hand, acetaldehyde selectivity over $CoFe_2O_4$ is significantly lower and with an opposite trend as a function of time, ranging from 17 to 28% at the beginning and after 20 min of ethanol exposure, respectively. The formation of acetaldehyde is likely due to the ethanol dehydrogenation/oxydehydrogenation reactions. Ethyl acetate represents the second most important reaction product, and the two spinels show similar selectivities (19% in cobaltite and 28% in ferrite at the end of the cycle). Notably, the selectivity to acetone over $CoFe_2O_4$ is in the range from 17 to 11%, while its selectivity over $FeCo_2O_4$ is much lower (<2%).

Fig. S10 and S11 show the conversion and the selectivity to the main products, obtained during the reduction step performed at 450°C for 20 min. Already at the beginning of the reaction, the ethanol conversion is quantitative and is stable during the reduction time for both oxides. One of the main products is hydrogen, with an initial selectivity of about 30% ($FeCo_2O_4$) and 51% ($CoFe_2O_4$), which increases up to 73 and 78%, respectively, at the end of the cycle. The trend observed for hydrogen very similar to that of CO_x and H_2O, suggesting that the prevailing reactions, which result in the oxide reduction, are the total and partial ethanol oxidation. Other by-products as acetaldehyde, acetone, ethyl acetate, ethylene and ethane were detected mainly at the beginning of the reduction. This means that the formation of these species is strongly connected to the presence of the spinel phases, whereas as soon as the mixed wüstite is formed their amount is strongly suppressed. This has

been confirmed by *in operando* investigation by XAS (see below).

After the 1st step with ethanol, the reduced material was then re-oxidized by water steam at 450°C during the same time on stream of 20 min, which corresponds to the 2nd step of the conventional two-step CLR process (Fig. S12, 13 and 14). Mass spectroscopy data indicate a significant difference in the amount of produced H_2 and CO_x gases over two spinels, which is proportional to the reduction extent of the solid together with its ability of being re-oxidized by means of H_2O. The higher hydrogen yield (~20 %) is obtained on $CoFe_2O_4$, whereas on $FeCo_2O_4$ its amount is 3-4 times lower (~5%). Beside the hydrogen production, the common feature for all the samples is the formation of CO_x (CO_2 and CO) during the re-oxidation step (Fig. S13 and S14), because of the gasification of carbonaceous residues, previously formed during the reduction step (see CHNS elemental analysis in Table S2 performed after the 1st step with ethanol).

CLR of ethanol: *in operando* XAS.

In order to have an atomic scale insight into the origin of the different chemical activity of the two spinels, *in operando* XAS measurements have been carried out under Chemical-Loop conditions. In particular, we have monitored the Fe K and Co K-edges during ethanol (20 minutes, 5.29% in nitrogen) or water (20 minutes, 8.31% in nitrogen) exposure at 450°C. The working temperature (450°C) was reached in inert atmosphere at 5°C/min, and XAS measurements were also acquired during the heating treatment. Fig. 6 shows the XANES and EXAFS spectra after each process step for both samples at the Fe K and Co K edges. After the thermal treatment, the oxidation states of Fe and Co in $FeCo_2O_4$ are almost unchanged, whereas a slight reduction of $CoFe_2O_4$ is evidenced by the decrease of the white line intensity at both edges, as well as by the shift of Fe K-edge energy toward lower values. This behavior could have two explanations: (i) cobaltite was synthesized at higher temperature than ferrite and, therefore, it is expected to be more stable; (ii) the particle size of cobaltite is larger than that of ferrite, therefore, cobaltite is less reactive. Moreover, the EXAFS peaks of both materials after annealing in inert atmosphere are less intense due to an increase of the disorder of the structures (high cation mobility) and to the noise induced by temperature and gas flow. EXAFS data suggest that the metal cations in tetrahedral environment are the most reactive species under these conditions, since the M_{octa}-M_{tetra} interactions suffer the largest drop in intensity. From the LCF analysis (Fig. S4, time=0 min), we can conclude that only a small fraction of $CoFe_2O_4$ (about 20%) and of $FeCo_2O_4$ (about 5%) are converted to a wüstite phase after the annealing in inert atmosphere.

In operando quick XAS spectra acquired during the following reduction and re-oxidation cycles (Fig. 6), confirm that the two spinels exhibit a rather different reactivity. After the first reduction cycle in ethanol atmosphere, $FeCo_2O_4$ is almost completely reduced: both the Fe K and Co K-edges XANES (Fig. 6a and 6b, and the corresponding LCF in Fig. S4) and EXAFS (Fig.
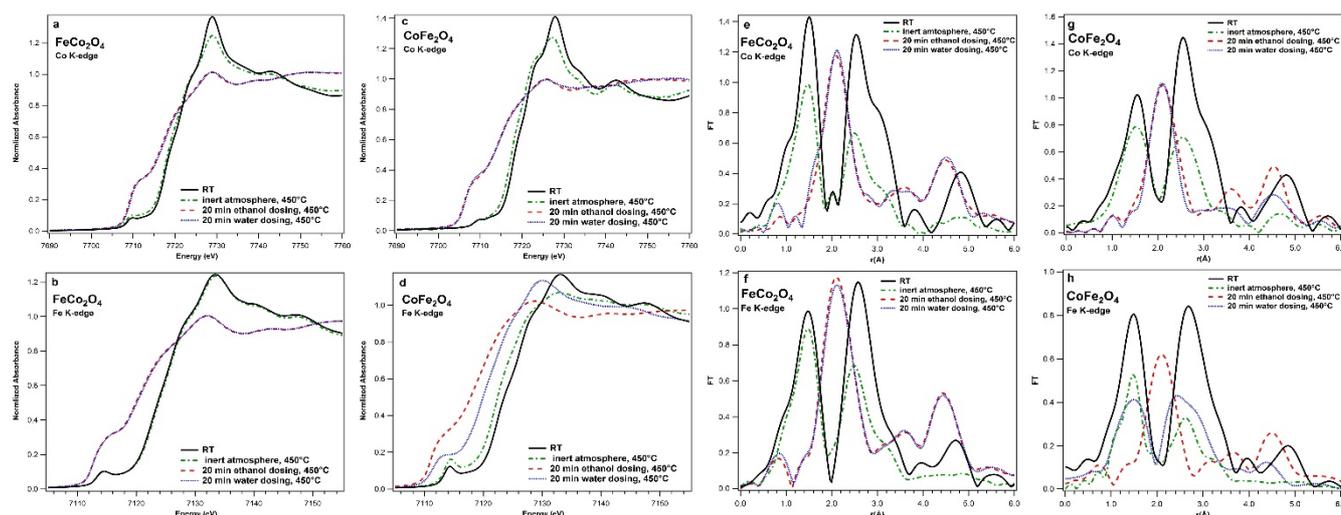
Fig. 6 XANES spectra at Co K-edge (a,c) and Fe K-edge (b,d) and Fourier transforms of $k^3\chi(k)$ at Co K-edge (e,g) and Fe K-edge (f,h) of FeCo$_2$O$_4$ (a,b,e,f) and CoFe$_2$O$_4$ (c,d,g,h) after three successive steps: annealing in inert atmosphere at 450°C, 20 minutes of ethanol dosing (0.08 ml/h) and 20 minutes of water dosing (0.04 ml/h).

6e and 6f) data confirm the formation of metal phases. The peak corresponding to M-O bonds disappears, whereas that corresponding to M-M in the metal phase appears. About 50 % of the iron cobaltite is rapidly converted (2 min) to a wüstite phase. This phase, however, has only a transient existence due to the fast reduction to the metal phase. The formation of metal Fe and Co starts as soon as some mixed wüstite phase is formed, and after 10 minutes reaches a plateau that corresponds to the conversion of about 85% of Co and 75% of Fe to metal alloy phases,[47]. Both cations are easily reduced; however, this tendency is higher for Co than for Fe, which in general requires a higher temperature and is more efficiently stabilized in the wüstite phase. Overall, the time evolution of the XANES spectra indicates that FeCo$_2$O$_4$ is rather unstable under reducing conditions and high temperature. Nonetheless, during the successive oxidation cycle with water vapor, the EXFAS spectra remain unchanged, indicating that the reduced phases are quite difficult to re-oxidize (Fig. 6a and 6b). This limited oxidation explains the low hydrogen yield detected during catalytic measurements for this material. Previous *in situ* X-ray Photoemission Spectroscopy (XPS) study on Co-Mn mixed spinel ferrites[27] on the other hand, indicate that the surface of these materials can be efficiently oxidized by water steam. This apparent contradiction can be solved considering the low surface area of FeCo$_2$O$_4$, and that XAS is a bulk technique. Moreover, it has been previously reported for other mixed spinels that the rate determining step of water oxidation is the diffusion of oxygen through the newly formed oxide layer.[48] Therefore, we can assume that a thin oxide passivation layer that can be hardly detected by XAS is formed on the metal surface and prevents further oxidation. On the other hand, CoFe$_2$O$_4$ is reduced to a mixed wüstite in first place and, subsequently, to a Co-Fe alloy. After 2 minutes in ethanol atmosphere, about 80% of Fe and 45% of Co are converted to a wüstite phase (Fig. S4). Interestingly, Co prefers to form a metal phase rather than a reduced Co(II) oxide, as demonstrated by the almost concurrent formation of CoO and Co metal. Fe,

instead, is quickly and almost quantitatively transformed into wüstite, which is only partially reduced to metal. This quantitative conversion of Fe is in contrast with the behavior of Fe in FeCo$_2$O$_4$, where was gradually converted both to metallic and wüstite phases. At the end of the cycle on CoFe$_2$O$_4$, the reduction of Fe to metal is only 60% to be compared with 90% for cobalt. It has been previously reported that the addition of Co to γ-Fe$_2$O$_3$, forming non-stoichiometric spinel, has a strong influence on its reduction properties. Pure iron oxide and spinels are reduced only to FeO, whereas the cobalt doped ferrite can be reduced up to Fe-Co alloys[18] During the subsequent oxidation process, Co is marginally oxidized by water (Fig. 6c and 6g); whereas Fe is clearly oxidized to a final oxidation state slightly higher than 2+ (Fig. 6d). The easier oxidation of iron is responsible for the higher yield of hydrogen on CoFe$_2$O$_4$ with respect to FeCo$_2$O$_4$. It should be highlighted that we have not found evidence (neither from EXAFS spectra nor from LCF of XANES data) of the formation of single metal spinels (Co$_3$O$_4$ or Fe$_3$O$_4$).

Combining XAS and catalytic tests: main results.

Overall, the body of our experimental data indicates that at high temperature (450°C) both spinels are highly active for the total decomposition of ethanol at 450ºC, producing H$_2$ and CO$_x$ as main products, whereas at 350°C the overall conversion decreases and other reaction paths, especially oxidative dehydrogenation, becomes relevant. The different Co/Fe ratio in the oxides is a key parameter for controlling their chemical activity. The cobalt rich spinel can be easily reduced, but it is very difficult to be re-oxidized by a mild oxidant as water. In contrast, a higher iron fraction makes the system more reversible since an intermediate iron wüstite phase, which is a better oxygen buffer, is stabilized.[49] Concerning the different selectivity in the anaerobic ethanol oxidation FeCo$_2$O$_4$ strongly favors the oxidative dehydrogenation to acetaldehyde with respect to CoFe$_2$O$_4$. The very high acetaldehyde yield observed at the beginning of the reaction can be traced back to very active tetrahedral species that are almost immediately

converted to less reactive octahedral divalent species. $CoFe_2O_4$ on the other hand shows a less pronounced selectivity toward acetaldehyde. In fact, it was suggested that a decrease of the amount of Fe(III) in tetrahedral sites in Co/Fe mixed spinel promotes dehydration rather than dehydrogenation.[50] Our data indeed, indicate that the ratio of Fe(III) in tetrahedral sites in the two spinels is inversely proportional to acetaldehyde selectivity. Another important parameter that controls the selectivity of the reaction is the type of majority carriers in the material:[51] n-type semiconductors can provide easily electron and favor dehydration, whereas the presence of mobile holes favors oxidative dehydrogenation. $CoFe_2O_4$ is an n-type semiconductor,[49] however upon reduction, it is converted to a wüstite-type oxide that is a p-type semiconductor. This change may explain why as a function of time the acetaldehyde selectivity increases for the cobalt ferrite.

Conclusion

By combining different characterization techniques (XRD, Raman and Mössbauer Spectroscopies), *in operando* Quick-EXAFS and catalysis measurements, we have investigated the structural and chemical properties of mixed Co-Fe spinels ($FeCo_2O_4$ and $CoFe_2O_4$) during each step of the CLR of ethanol. Firstly, we have studied the freshly prepared materials and we have determined the oxidation state of Fe and Co and the inversion parameter γ in the two structures (0.8 and 0.6 for $CoFe_2O_4$ and $FeCo_2O_4$, respectively). Then, by means of *in operando* Quick-EXAFS measurements, we have followed in real time the solid state redox processes of these mixed spinels as a response to temperature and reactive atmosphere. In particular, we monitored the reduction of the catalysts during the first step of CLR of ethanol and the oxidation during H_2O steam exposure. These structural data were combined with the analysis of the reaction products in order to identify which are the most chemically active cations inside the spinel structure and what parameters control the chemical activity toward ethanol decomposition. These experiments have highlighted the influence of both coordination and chemical nature of the cations on the catalytic properties. The cations in tetrahedral sites of the spinel structure show a higher reducibility with the respect of octahedral ones, independently from their chemical nature. The reduction of the spinel structure leads to the formation of a wüstite phase and of FeCo metal alloys. Conversely, considering the ratio between reduced phases (wüstite and metal alloy), the chemical nature of the cation plays an important role. In fact, the total reduction of Co to Co(0) is faster with respect to that of Fe. This is reflected in the oxidation step of CLR, where the re-oxidization of cobaltite by a mild oxidant such as water is practically ineffective. This different behavior influences the ethanol decomposition selectivity and yield. At mild temperature (350°C) $FeCo_2O_4$ strongly favors the oxidative dehydrogenation to acetaldehyde with respect to $CoFe_2O_4$. Moreover, the very high acetaldehyde yield observed at the beginning of the reaction can be traced back to very active tetrahedral species that are almost immediately converted to less reactive octahedral divalent

species. At higher temperature (450°C), both spinels are almost totally reduced to metal phases and are highly active for the total decomposition of ethanol, producing H_2 and CO_x as main products.

In conclusion, our study indicate that $CoFe_2O_4$ is a more promising material than $FeCo_2O_4$ for CLR due to a more reversible chemistry connected to the better stability of the wüstite phase. Nonetheless, the fundamental knowledge acquired in this study may be a stepping stone for the design of new improved materials to be used as solid oxygen carriers and novel catalysts for the selective oxidation of alcohols.

Experimental

Synthesis of spinel oxides

$CoFe_2O_4$ was synthesized using the co-precipitation method reported by Vozniuk et al.[27] Briefly, a solution containing metal nitrate precursors in the desired molar ratios was drop-by-drop added into the reaction vessel containing 0.5 L of 2 M NaOH (Sigma-Aldrich) aqueous solution at 50°C under vigorous stirring. The suspension was stirred for 2 h at 50°C keeping the pH above 13 by adding a 3M NaOH solution if necessary. The precipitate was separated by vacuum filtration, washed with distilled water and dried at 120°C. Finally, the solid material was calcined in static air at 450°C for 8h with the heating rate of 10°C min^{-1}. $FeCo_2O_4$ was synthesized following a recipe previously reported in literature.[28] Briefly, iron chloride ($FeCl_3 \cdot 6H_2O$, Sigma-Aldrich) and cobalt chloride ($CoCl_2 \cdot 6H_2O$, Sigma-Aldrich), with a Co:Fe molar ratio of 2:1 , were dissolved in distilled water and poured into a boiling 2M KOH solution under vigorous stirring at 80°C for 1 hour. After repeated filtering and washing with boiling distilled water, the resulting power was dried at 120°C and then calcined at 900°C for 17h with a heating rate of 5°C min^{-1}.

Materials characterization

In operando Quick EXAFS measurements were carried out in transmission mode at the Fe K and Co K edges at the ROCK beamline (SOLEIL synchrotron, France). The Quick-EXAFS monochromator (equipped with a Si(111) channel-cut crystal) operated at an oscillation velocity of 2 Hz. The detectors were ionization chambers. The samples in powder form were diluted with boron nitride (mass ratio=1:1.2) and inserted into quartz capillaries (diameter=1.5 mm, wall thickness=0.03 mm). The capillaries were centered perpendicularly to the X-ray beam and connected to a heated gas line. The samples were heated at the desired temperature (from RT to 500°C) by a heating gun. During the annealing in reductive atmosphere (from RT to 500°C, 5°C min-1), ethanol was dosed using a syringe pump and nitrogen as carrier gas (0.69% of ethanol in N2). During chemical loop reforming (CLR) of ethanol, the samples were heated at the desired temperature (350 or 450°C) in inert atmosphere. Then ethanol and water were dosed alternatively (20 or 40 minutes steps) using syringe pumps and nitrogen as carrier gas. EXAFS spectra were continuously acquired during these processes. The corresponding metal foils were measured simultaneously and

used to calibrate and align the spectra. Pellets of the various oxide standards were measured in transmission mode at RT.

Powders were characterized by P-XRD in a Philips X'Pert X'Celerator, with Cu-kα radiation in a 2θ range between 5-80° with step of 0.1°.

Characterization by Raman spectroscopy was performed using a ThermoFisher DXR Raman microscope. The spectra were recorded using a laser with an excitation wavelength of 532 nm (5 mW), focused on the sample with a 50× LWD objective (Olympus).

Reactivity experiments were carried out by loading 400 mg of the pelletized sample (with particles diameter ≈0.25 to 0.6 mm) in the fixed-bed quartz flow reactor with an internal diameter of 12 mm and a length of 30 cm. The products were monitored on-line by an Agilent 3000A micro-GC.

Further details about XAS data analysis procedures, catalytic tests and Mössbauer spectroscopy are reported in the supporting information.

Conflicts of interest

There are no conflicts to declare.

Acknowledgements

Notes and references

1   M. B. Gawande, R. K. Pandey, R. V. Jayaram, *Catal. Sci. Technol.* 2012, **2**, 1113-1125.
2   C. Yuan, H. B. Wu, Y. Xie, X. W. D. Lou, *Angew. Chem. Int. Ed.* 2014, **53**, 1488-1504.
3   J. H. Clark, *Green Chem.* 1999, **1**, 1-8.
4   Y. Liu, G. Zhao, D. Wang, Y. Li, *Natl Sci Rev* 2015, **2**, 150-166.
5   A. Chieregato; J. M. López Nieto; F. Cavani, *Coord. Chem. Rev*. 2015, **301–302**, 3–23.
6   V, Polshettiwar, B. Baruwati,; R. S. Varma, *ACS Nano* 2009, **3**, 728-736.
7   V. E. Henrich, P. A. Cox, *Cambridge Univ. Press* 1994.
8   M. R. N. S. Hamdani, R. N. Singh, P. Chartier, *Int. J. Electrochem. Sci* 2010**, 5**, 556-577.
9   K. E. Sickafus, J. M. Willis, N. W. Grimes, *J. Am. Ceram. Soc*. 1999, **82**, 3279–3292
10 S. Permien, S. Indris, U. Schürmann, L. Kienle, S. Zander, S. Doyle, W. Bensch, *Chem. Mater.* 2016, **28**, 434– 444.
11 C. Wei, Z. Feng, G. G. Scherer, J. Barber, Y. Shao-Horn, Z. J. C Xu, Adv. Mater. 2017, **29**, 1606800.

12 X. Wang, Y. Liu, T. Zhang, Y. Luo, Z. Lan, K. Zhang, J. Zuo, L. J. R. Wang, *ACS Catal.* 2017, **7** , 1626–1636.
13 H. Zhu, S. Zhang, Y. X. Huang, L. Wu, S. Sun, *Nano letters* 2013, **13**, 2947-2951.
14 T. Maiyalagan, K. A. Jarvis, S. Therese, P. J Ferreira, A. Manthiram, *Nat. commun.* 2014, **5**, 3949.
15 X. Xie, Y. Li, Z. Q. Liu, M. Haruta, W. Shen, *Nature* 2009, **458**, 746-749.
16 F. F. Tao, J. J Shan, L. Nguyen, Z. Wang, S. Zhang, L. Zhang, L. Zhang, Z. Wu, W. Huang, S. Zeng P.Hu, *Nat. commun.* 2015, **6***, 7798.
17 P. Cho, T. Mattisson, A. Lyngfelt, *Fuel*, 2004, **83**, 1215-1225.
18 R. J. Scheffe, M. D. Allendorf, E. N. Coker, B. W Jacobs, A. H.McDaniel, A. W Weimer. *Chem Mater.* 2011**, 23***, 2030-2038
19 C. Trevisanut, M. Mari, J. M. M. Millet, F. Cavani, *Int. J. Hydrogen Energy* 2015, **40**, 5264-5271.
20 V. J. Aston, B. W. Evanko, A. W. Weimer, Int. J. Hydrogen Energy 2013, **38**, 9085-9096.
21 G. Voitic, V. Hacker. *RSC Adv.* 2016**, 6** (100), 98267-98296.
22 Z. Ma, L. Ren, S. Xing, Y. Wu, Y. Gao. *J. Phys. Chem. C*, 2015, **119** (40), 23068–23074.
23 Zhou X., Huang J., Zhang F.M., Zhao Y., Zhang Y., Ding Y.. *Dalton Trans.* 2017**,** 10.1039/C7DT00302A
24 M. Nasrollahzadeh, M. Bagherzadeh, H. Karimi, *J. Colloid Interface Sci.* 2016, **465**, 271–278.
25 H. Jin, T. Okamoto, M. Ishida, Enery Fuels 1998**, 12**, 1272– 1277
26 E. Hormilleja, P. Durán, J. Plou, J. Herguido, Peña J.A. *Int. J. of Hydrogen Energy* 2014, **39**, 5267-5273.
27 O. Vozniuk, S. Agnoli, L. Artiglia, A. Vassoi, N. Tanchoux, F. Di Renzo, G. Granozzi, F. Cavani, *Green Chem.* 2016, **18**, 1038-1050.
28 T. A. S. Ferreira J. C. Waerenborgh M. H. R. M. Mendonça, M. R. Nunes, F. M. Costa, *Solid State Sciences* 2003, **5**, 383–392.
29 E. Manova, T. Tsoncheva, D. Paneva, I. Mitov, K. Tenchev, L. Petrov, *Applied Catalysis A: General* 2004, **277**, 119–127.
30 P. Chandramohan, M. P. Srinivasan, S. Velmurugan, S. V. Narasimhan, *J. Solid State Chem.* 2011, **184**, 89–96.
31 O. Vozniuk, C. Bazzo, S. Albonetti, N. Tanchoux, J.-M. M Millet, F. Bosselet, F. Di Renzo, F. Cavani *ChemCatChem* **2017**, DOI: 10.1002/cctc.201601605R1
32 D. Carta, M. F. Casula, A. Falqui, D. Loche, G. Mountjoy, C. Sangregorio, A. Corrias, *J. Phys. Chem. C,* 2009, 113 (20), 8606–8615.
33 V. Krishnan, R. K. Selvan, C. O. Augustin, A. Gedanken, H. Bertagnolli, *J. Phys. Chem. C* 2007, **111** (45), 16724–16733.
34 M. H. Nilsen, C. Nordhei, A. L. Ramstad, D.G. Nicholson, *J. Phys. Chem. C* 2007, **111** (17), 6252–6262.
35 G. A. Sawatxky, F. Van Der Woude, A. H. Morrish, *P Phys. Rev*. 1969, **187**, 747.
36 D. Carta, A. Corrias, G. Navarra, *Journal of Non-Crystalline Solids* 2011, **357**, 2611–2614.
37 Z. G. Lu, J. H. Zhu, Z. H. Bi, X. C. A Lu, *J. Power Sources* 2008, **180**, 172– 175.
38 Y. I. Ustinovshikov, P, B. E. Ushkarev, I. V. Sapegina, *Inorg. Mater.* 2006, **42**, 354– 359.
39 V. Crocellà, F. Cavani, G. Cerrato, S. Cocchi, M. Comito, G. Magnacca, C. Morterra, *J. Phys. Chem. C*, 2012, **116**, 14998–15009.
40 Y. Tamaura, M. Kojima, T. Sano, Y. Ueda, N. Hasegawa, M. Tsuji, *International Journal of Hydrogen Energy*, 1998, **23**(12), 1185-1191.
41 M. Tabata, K. Akanuma, T. Togawa, M. Tsuji, Y. Tamaura, *J Chem Soc Faraday Trans* 1994, **90**, 1171.
42 W. C. Cho, C. G. Kim, S. U. Jeong, K. S. Kang, S. D. Kim, *Industrial & Engineering Chemistry Research* 2015, **54** (12), 3091-3100.
43 I. Barin, O. Knacke, Springer-Verlag: Berlin, 1973, 66-74.
44 C. D. Bohn, C. R Muller, J. P Cleeton, A. N. Hayhurst, J. F. Davidson, S. A Scott, J. S. Dennis, *Ind. Eng. Chem. Res.* 2008, **47,** 7623– 7630.
45 S. Liu, F. He, Z. Huang, A. Zheng, Y. Feng, Y. Shen, H. Li, H. Wu, P. Glarborg, *Energy Fuels* 2016, **30,** 4251–4262.
46 M. D.Allendorf. *Energy & Fuels* 2008, **22**, 4115–4124.
47 T. Block, N. Knoblauch, M. Schmücker, *Thermochim. Acta* 2014, **577**, 25– 32.
48 K. S. Go, S. R Son, S. D. Kim, *Int. J. Hydrogen Energy* 2008, **33**, 5986-5995.
49 N. Bahlawane, PH. Ngamou, V. Vannier, T. Kottke, J. Heberle, K. Kohse-Höinghaus, *Phys. Chem. Chem. Phys.* 2009, **11**, 9224–9232.
50 G. R. Dube, V. S. A Darshane, *Bull.Chem.Soc.Jpn* 1991, **64**, 2449-2543.
51 O. V. Krylov, E. M. Loebl, *Physical Chemistry: A Series of Monographs* 1970**, 17.**